Original Article

A postmortem high-resolution MRI study of the development of cochlear nerve-related structures in the second and third trimesters of pregnancy

Hui Zhao[1]^, Lixin Sun[1]^, Lianxiang Xiao[2]^, Linsheng Wang[1]^, Na Hu[1]^, Mingming Miao[3]^, Daniel Thomas Ginat[4], Carlo A. Mallio[5,6], Xiangtao Lin[7]^

[1]Department of Radiology, Shandong Provincial ENT Hospital, Shandong University, Jinan, China; [2]Department of Radiology, Maternal and Child Health Care Hospital of Shandong Province, Jinan, China; [3]Department of Radiology, The Fifth People's Hospital of Jinan, Jinan, China; [4]Department of Radiology, Section of Neuroradiology, University of Chicago, Chicago, IL, USA; [5]Fondazione Policlinico Universitario Campus Bio-Medico, Rome, Italy; [6]Research Unit of Radiology, Department of Medicine and Surgery, Università Campus Bio-Medico di Roma, Rome, Italy; [7]Department of Radiology, Shandong Provincial Hospital, Shandong University, Jinan, China

Contributions: (I) Conception and design: H Zhao, X Lin; (II) Administrative support: L Sun, L Wang; (III) Provision of study materials or patients: L Xiao; (IV) Collection and assembly of data: N Hu, M Miao; (V) Data analysis and interpretation: H Zhao; (VI) Manuscript writing: All authors; (VII) Final approval of manuscript: All authors.

Correspondence to: Xiangtao Lin, MD, PhD. Department of Radiology, Shandong Provincial Hospital, Shandong University, No. 324 Jingwu Road, Jinan 250021, China. Email: linxt616@163.com.

Background: Magnetic resonance imaging (MRI) is used to determine whether cochlear nerve development is normal in infants and adults, but it has not yet been used to evaluate cochlear nerve development or measure cochlear nerve-related structures in the fetus. This study sought to provide imaging data for clinical evaluations concerning cochlear nerve development in the fetus using MRI.

Methods: Postmortem 3.0-Tesla MRI of inner ear was performed in 51 fetuses with normal temporal bones at 25 to 40 weeks of gestation. The continuous scanning protocol incorporated axial three-dimensional (3D) sampling perfection with application-specific contrasts using different flip angle evolution sequences. The images were evaluated to measure the structures of the cochlear aperture (CA), internal auditory canal (IAC), and vestibulocochlear and facial nerves in the cerebellopontine angle (CPA), which have been reported to be associated with cochlear nerve development. We also calculated the ratio between the diameters of the vestibulocochlear and facial nerves. The measurable parameters were compared between the right and left sides. The threshold for statistical significance was set at $P<0.05$.

Results: The inner ear anatomy was discernible on MRI in all the fetal specimens, and growth of the CA, IAC, vestibulocochlear nerve, and facial nerve in the CPA was observed as fetal age increased. There was no significant difference in the measurements of these structures between the right and left sides (all $P>0.05$).

Conclusions: MRI can be used to help evaluate the anatomy and development of the cochlear nerve in the fetus. These normative measurements could be valuable for clinical evaluations of the cochlear nerve.

Keywords: Fetus; postmortem; magnetic resonance imaging (MRI); cochlear nerve; development

Submitted Mar 27, 2024. Accepted for publication Jul 09, 2024. Published online Aug 12, 2024.
doi: 10.21037/qims-24-626
View this article at: https://dx.doi.org/10.21037/qims-24-626

^ ORCID: Hui Zhao, 0000-0003-3215-7939; Lixin Sun, 0000-0002-8831-6012; Lianxiang Xiao, 0000-0002-1771-8698; Linsheng Wang, 0000-0002-6893-0322; Na Hu, 0000-0003-4252-1449; Mingming Miao, 0009-0004-8154-4815; Xiangtao Lin, 0000-0003-3251-7939.

Introduction

Cochlear nerve deficiency includes cochlear nerve aplasia and cochlear nerve hypoplasia, which are typically associated with congenital sensorineural hearing loss (1,2). Cochlear nerve deficiency accounts for approximately 10–19% of hearing loss cases in children (3). Therefore, it is important to determine whether the cochlear nerve is abnormal or not. Currently, the accurate diagnosis of cochlear nerve deficiency is a research hotspot.

As the external ear, middle ear, and inner ear develop independently, inner ear malformations are often isolated without external and middle ear abnormalities. Moreover, due to the relatively deep positioning of the inner ear, it is difficult to make an accurate diagnosis by prenatal ultrasound (4). Fetal magnetic resonance imaging (MRI) is a commonly performed alternative prenatal imaging modality that is critical for evaluating normal fetal anatomy, congenital malformations, and abnormal development, and for understanding fetal organ functions and metabolic activity (5). Notably, in fetal cranial examinations, the coronal position parallel to the brainstem scan symmetrically displays the bilateral inner ear structure (6). Therefore, MRI of the fetal inner ear can be used to rule out inner ear abnormalities. However, MRI studies on the fetal ear have predominantly focused on the middle ear (7,8) and external ear (9,10). The few studies that have investigated the inner ear are mostly case studies (11). Additionally, due to the limited resolution of MRI in intrauterine fetuses, the fine anatomical structure of the inner ear cannot be adequately depicted, and it is difficult to see the delicate cochlear nerve clearly.

Postmortem MRI has also been used to investigate fetal temporal bones development (12,13), as it allows the details of the inner ear to be clearly identified. However, while the development of the cochlear nerve can be directly assessed by measuring its diameter, due to resolution limitations, the cochlear nerve cannot be clearly observed in many cases, even on specimen MRI scans. The vestibulocochlear and facial nerves in the cerebellopontine angle (CPA) (14,15), internal auditory canal (IAC) (16,17), and cochlear aperture (CA) (18,19) indirectly reflect the development of the cochlear nerve. Nevertheless, only limited research appears to have been conducted on the development of the cochlear nerve and the measurement of the structures related to it. MRI scanning of the temporal bone of 18 fetal specimens in 1996 clearly visualized the inner ear structure; however, only morphological observations (without MRI measurements) were obtained (12). Therefore, to illustrate the fetal inner ear structure and explore the MRI manifestations of inner ear development, we used the 3.0-Tesla MRI system to scan 51 fetal specimens at 25 to 40 weeks of gestation. To establish the standard measurement range of the fetal inner ear, the diameters of the CA, IAC, and vestibulocochlear and facial nerves in the CPA were measured. These results could potentially serve to guide clinical evaluations of cochlear nerve development in fetuses.

Methods

Fetal specimens

A total of 51 fetus specimens from 25 to 40 weeks of gestation were included in this study. All the postmortem fetuses were obtained from the School of Medicine, Shandong University, Research Center for Sectional and Imaging Anatomy. These specimens had previously been collected from hospitals in the Shandong Province of China, and were partially used to study the fetal spine, sacrococcygeal centrum ossification centers, the fetal thymus, and the fetal spinal canal and spinal cord in previous publications (20-23).

The cohort comprised 30 male and 21 female fetuses. Some specimens were acquired following medically indicated abortions due to maternal teratogenesis infection, stressful intrauterine conditions, pregnancy-induced hypertension syndrome, severe cardiovascular disease, chronic nephritis, and stillbirth caused by accident. The other specimens were collected from spontaneous abortions due to unknown causes, which might have been related to uterine myoma, systemic infection, or neuro-psychentonia. The gestational week (GW), gender, and reason for the termination of pregnancy for each specimen in the study cohort are listed in *Table 1*. The parents provided informed consent for the donation of the fetal cadavers. The study protocol was approved by the Ethics Committee at the School of Medicine, Shandong University (No. SDULCLL2021-1-05). The study was conducted in accordance with the Declaration of Helsinki (as revised in 2013).

Fetal gestational age (GA) was estimated based on the date of the mother's last menstrual period and the length of the crown-rump region of the fetus. The inclusion criteria for the study were as follows: (I) a lack of intrauterine growth restriction, chromosomal abnormalities, or any other intrauterine stressors; (II) no family history of genetic

Table 1 The demographic information of the specimens

GW	Number (n=51)	Gender (M/F)	Reason for termination of pregnancy
25	5	3/2	SA [3], CN [1], SCD [1]
26	4	2/2	SA [3], SCD [1]
27	5	3/2	SA [3], SCD [1], TI [1]
28	3	3/0	SA [2], PIHS [1]
29	3	2/1	SCD [2], TI [1]
30	2	1/1	SIC [1], SCD [1]
31	3	1/2	SIC [1], PIHS [1], SCD [1]
32	2	0/2	SCD [1], CN [1]
33	3	1/2	PIHS [1], SCD [1], SCA [1]
34	3	2/1	SIC [1], PIHS [1], CN [1]
35	1	1/0	PIHS [1]
36	3	1/2	PIHS [1], CN [1], SCA [1]
37	4	3/1	PIHS [3], CN [1]
38	2	2/0	PIHS [1], SCD [1]
39	3	3/0	PIHS [1], CN [1], SCA [1]
40	5	2/3	PIHS [2], SCD [1], CN [1], SCA [1]

GW, gestational week; M, male; F, female; SA, spontaneous abortion; CN, chronic nephritis; SCD, severe cardiovascular disease; TI, teratogenesis infection; PIHS, pregnancy-induced hypertension syndrome; SIC, stressful intrauterine condition; SCA, stillbirth caused by accident.

disorders associated with chromosomal abnormalities or deafness genes for the past three generations; and (III) normal temporal bone development during the intrauterine ultrasound and postmortem MRI. All the fetal specimens were refrigerated (at approximately −26 to −18 ℃) within 48 hours of delivery. The MRI examinations were performed at room temperature (at approximately 26 ℃).

MRI

All the scans were performed with a 3.0-Tesla MRI system (MAGNTOM Prisma, Siemens Healthcare, Germany) fitted with a 64-channel array head and neck coil. The temporal bone was covered using three-dimensional (3D) T2-weighted sampling perfection with application-specific contrasts using different flip angle evolution (T2-SPACE) sequence. The parameters of the 3D T2-SPACE sequence were as follows: plane = axial; field of view =160 mm × 160 mm; repetition time =1,200 ms; echo time =125 ms; slice thickness =0.5 mm with no slice intervals; voxel size =0.5 mm × 0.5 mm × 0.5 mm; and excitations =1.6. The average total scan time was approximately 2 min and 41 s.

Image processing and analysis

The MRI scans were saved in Digital Imaging and Communications in Medicine (DICOM) format and transmitted to the GE AW4.7 workstation (Discovery CT 750 HD) for multi-plane image reconstruction. The MRI images were independently reviewed by two radiologists with more than five years of experience each in fetal MRI (N.H. and M.M.). These radiologists were blinded to the imaging findings. In cases of differing opinions, consensus was reached through discussion. To determine the final measurement result, the area of interest was magnified four times. Each parameter was manually measured twice, and the average value was calculated. The following parameters were measured:

(I) The vestibulocochlear and facial nerve diameters of the CPA, which were measured from an oblique sagittal reconstruction image perpendicular to the inner ear canal (*Figure 1*). The average values of the anteroposterior diameter along with the craniocaudal diameter were also obtained and their ratios calculated.

(II) The IAC diameters and lengths in the axial and coronal planes. The mean of the distance from the falciform crest to the hilar region of the inner ear measured in the coronal and axial views was defined as the length of the IAC. Anteroposterior and craniocaudal diameters were obtained from the axial and coronal IAC images (*Figure 2*). The shape of the IAC was also observed.

(III) The CA diameter. First, the CA was displayed on the axial image with the sagittal alignment line parallel to the CA. Next, the CA was displayed on the sagittal image, and the axial image was reconstructed to show the CA maximum diameter plane (*Figure 3*).

Statistical analysis

All the statistical analyses were performed using SPSS 22.0 (IBM, Armonk, NY, USA). The data were presented as the mean ± standard deviation of the measurements. We used the inter-class correlation coefficient (ICC) to test

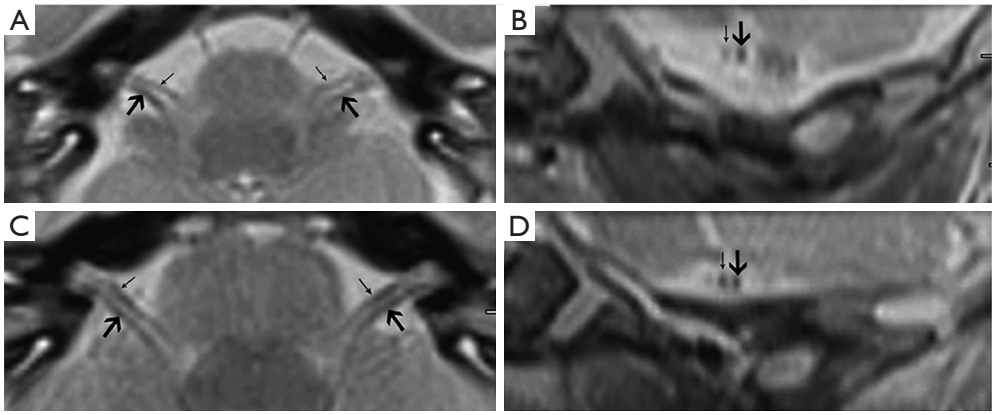

Figure 1 Facial nerve and vestibulocochlear nerve in the CPA at 28 weeks of gestation (A,B) and 35 weeks of gestation (C,D). (A,C) Transverse 3D SPACE T2-weighted scans of the facial nerve (thin arrow) and vestibulocochlear nerve (thick arrow) in the CPA. The nerves are parallel with the facial nerve in the front and the vestibulocochlear nerve in the back. (B,D) Oblique sagittal image showing the facial nerve (thin arrow) anteriorly and the vestibulocochlear nerve (thick arrow) posteriorly. CPA, cerebellopontine angle; 3D, three-dimensional; SPACE, sampling perfection with application-specific contrasts using different flip angle evolution.

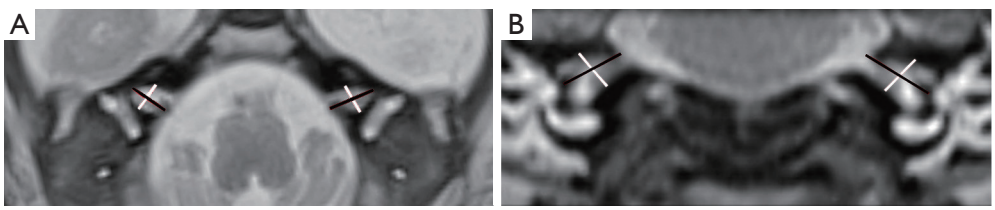

Figure 2 The IAC was measured in the axial and coronal 3D SPACE T2-weighted MRI images. (A) The anteroposterior diameter (white line) and length (black line) of the IAC were measured in the axial image at 30 weeks of gestation. (B) The craniocaudal diameter (white line) and length (black line) of the IAC were measured in the coronal image at 36 weeks of gestation. IAC, internal auditory canal; MRI, magnetic resonance imaging; 3D, three-dimensional; SPACE, sampling perfection with application-specific contrasts using different flip angle evolution.

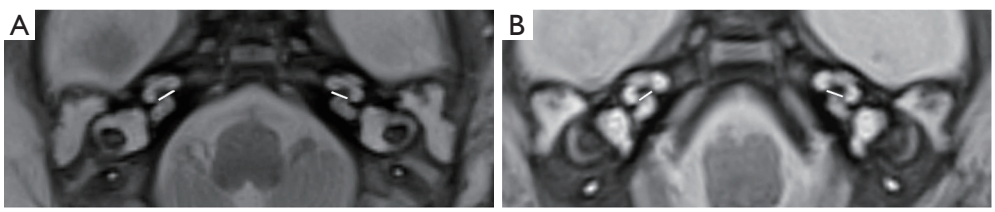

Figure 3 The diameter of the CA was measured at the maximum level of the CA in the axial 3D SPACE T2-weighted MRI images. (A) The diameter of the CA at 32 weeks of gestation (white line). (B) The diameter of the CA at 29 weeks of gestation (white line). CA, cochlear aperture; 3D, three-dimensional; SPACE, sampling perfection with application-specific contrasts using different flip angle evolution; MRI, magnetic resonance imaging.

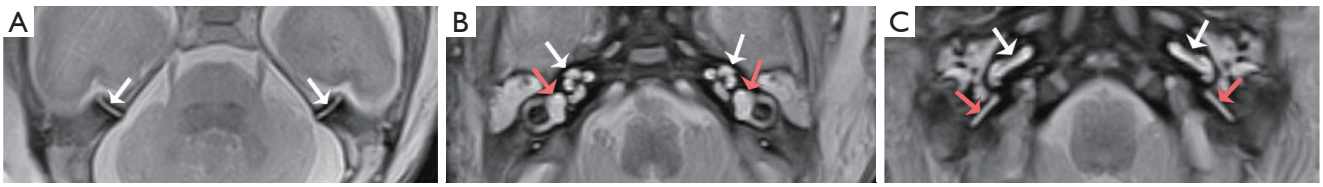

Figure 4 Axial 3D SPACE T2-weighted MRI images showing the inner ear structures at 34 weeks of gestation. (A) The right and left superior semicircular canals (white arrow). (B) The cochlear top and middle turn (white arrow) and the vestibule (red arrow). (C) The cochlear basal turn (white arrow) and posterior semicircular canal (red arrow). 3D, three-dimensional; SPACE, sampling perfection with application-specific contrasts using different flip angle evolution; MRI, magnetic resonance imaging.

the measurement consistency between the two viewers. Additionally, we employed the paired-sample *t*-test to compare the two groups. Spearman's correlation coefficient was applied to identify any correlation between the measurement results and GWs. A P value <0.05 was considered statistically significant.

Results

This study included 51 fetal specimens (30 males and 21 females, at 25–40 weeks of gestation). The GA, calculated based on the crown-rump length, was highly correlated with that calculated using the known date of the beginning of the mother's last maternal menstrual period (R=0.97; P<0.001).

The first morphological observation (i.e., the 3D T2-SPACE sequence images) depicted the following inner ear structures in the second and third trimesters: cochlea, CA, vestibule, semicircular canal, IAC, and vestibulocochlear and facial nerves in the CPA (*Figure 4*). The IAC was variable in shape, and roughly categorized as parallel, flared, or ampulla tubes. The IAC length was correlated with the GA (*Figure 5*).

As the scatterplots show (*Figure 6A-6E*), the diameters of the vestibulocochlear and facial nerves in the CPA, as well as the diameters of the IAC in both the axial and coronal planes, and the diameter of the CA, remained consistent throughout the second and third trimesters of pregnancy. Indeed, only the length of the IAC in both the axial and coronal planes exhibited a linear increase with GA (left in axial planes: R^2=0.78, P<0.05; right in axial planes: R^2=0.78, P<0.05; left in coronal planes: R^2=0.71, P<0.05; right in coronal planes R^2=0.67, P<0.05) (*Figure 6F,6G*). The visibility of the inner ear anatomy improved as the fetal age increased.

The average diameter of the vestibulocochlear and facial nerve diameters in the CPA, the diameters and lengths of the IAC in both the axial and coronal planes, and the diameter of the CA were 1.00±0.14, 0.70±0.13, 3.64±0.57, 3.55±0.1.27, 4.07±0.52, 4.12±1.11, and 1.90±0.17 mm, respectively. The results showed that there was strong consistency in the measurements of these cochlear nerve-related structures (ICC: 0.73–0.94; *Table 2*).

Table 3 summarizes the MRI data for these cochlear nerve-related structures. No significant differences were observed between the measurable parameters of these cochlear nerve-related structures on the left and right sides.

Discussion

We found that the high-resolution 3D T2-SPACE sequence could be used to visualize the inner ear structures of postmortem fetal specimens. Several structures, including the cochlea, CA, vestibule, semicircular canal, IAC, and nerves in the CPA became more visible as the GA increased. Imaging-based measurements were taken to preliminarily determine the expected values of the structures related to cochlear nerve development. The measurement indices did not differ significantly between the two sides. The measurements of the diameters of these structures provided quantitative data on the inner ear growth of the fetuses between 25 to 40 weeks of gestation and further reflected the development of the cochlear nerve.

Fetal movement is the main factor affecting MRI imaging. Due to issues related to the safety of pregnant women and fetuses, sedatives cannot be used during the scanning process; thus, only fast-imaging sequences can be used to reduce the interference of fetal movement artifacts. However, as the current scanning technology cannot sufficiently display the fine structure of the inner ear, it fails to meet clinical requirements. To study the development of the fetal cochlear nerve, it is necessary to establish new

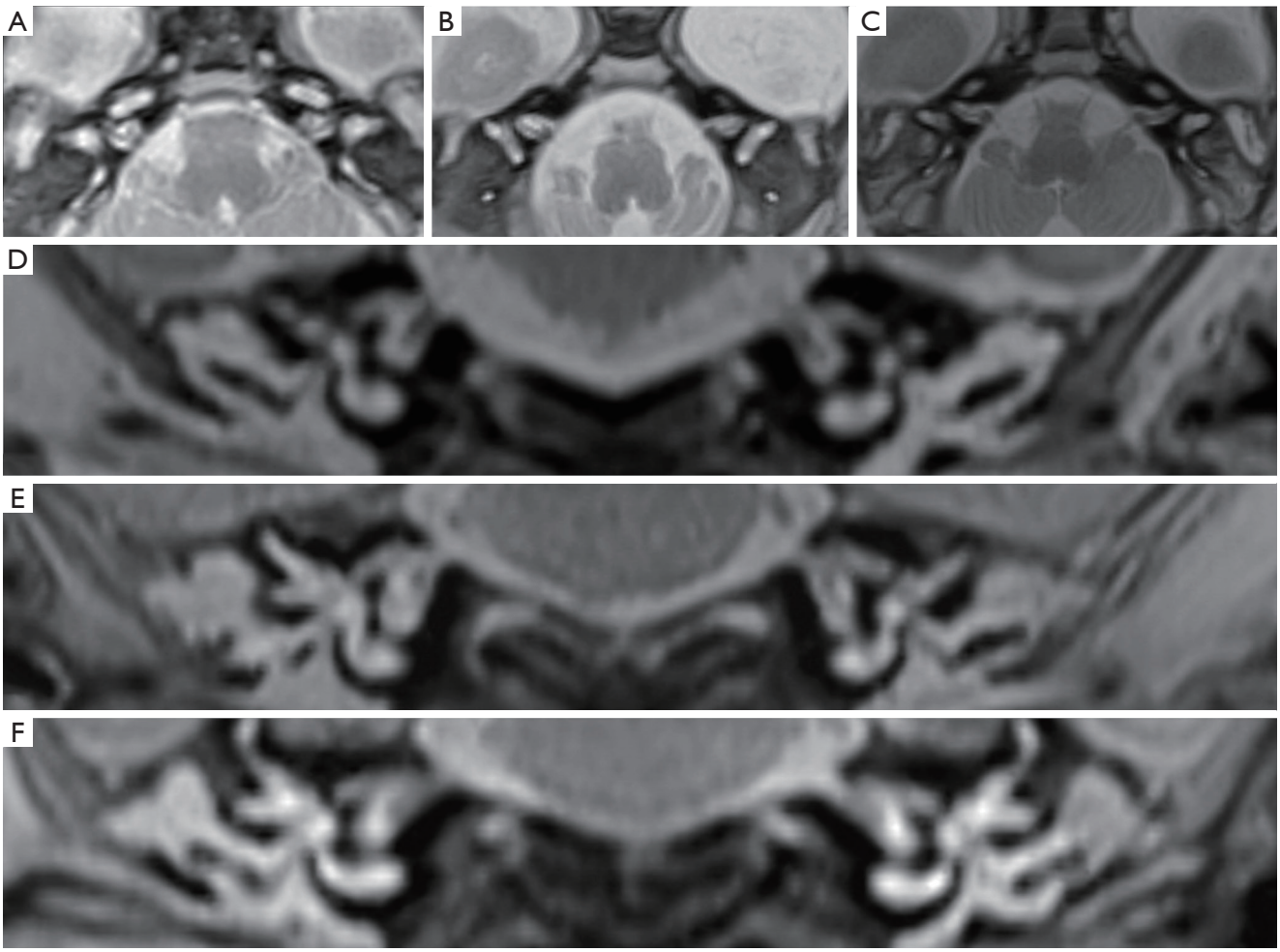

Figure 5 The IAC at 24 weeks of gestation (A,D), 30 weeks of gestation (B,E), and 36 weeks of gestation (C,F). (A-C) Axial 3D SPACE T2-weighted MRI image showing the right and left IAC; the length of the IAC increased as the GA increased. (D-F) Coronal 3D SPACE T2-weighted MRI showing the bilateral IAC; the length of the IAC increased as the GA increased. The IAC is divided into two parts at the bottom, each of which consists of fine nerves, one leading to the cochlea and the other leading to the vestibule. IAC, internal auditory canal; 3D, three-dimensional; SPACE, sampling perfection with application-specific contrasts using different flip angle evolution; MRI, magnetic resonance imaging; GA, gestational age.

methods for the in-depth exploration of the inner ear anatomy.

MRI of fetal specimens is not limited by the field strength or scanning time; moreover, a high-resolution isotropic scanning sequence can be used to obtain high-definition images and perform multi-level reconstruction, which is convenient for fetal scientific research. Nevertheless, the quality of specimen MRI images is susceptible to various influential factors, including the acquisition temperature, formalin immersion duration, and specimen storage time. Temperature also affects the MRI signal intensity and image contrast. At temperatures below 20 ℃, the T2-weighted MRI images contrast is reduced to a certain extent and the signal intensity changes (24,25). To mitigate the influence of chemical reactions, such as tissue dehydration and protein cross-linking, which can potentially change the relaxation time (26), the cadavers used in this study underwent frozen preservation. Further, to minimize the detrimental effects of prolonged storage on image clarity, the MRI scanning was completed within one month from the time of delivery. Notably, a previous study showed that the quality of frozen-thawed MRI images is similar to that of MRI images

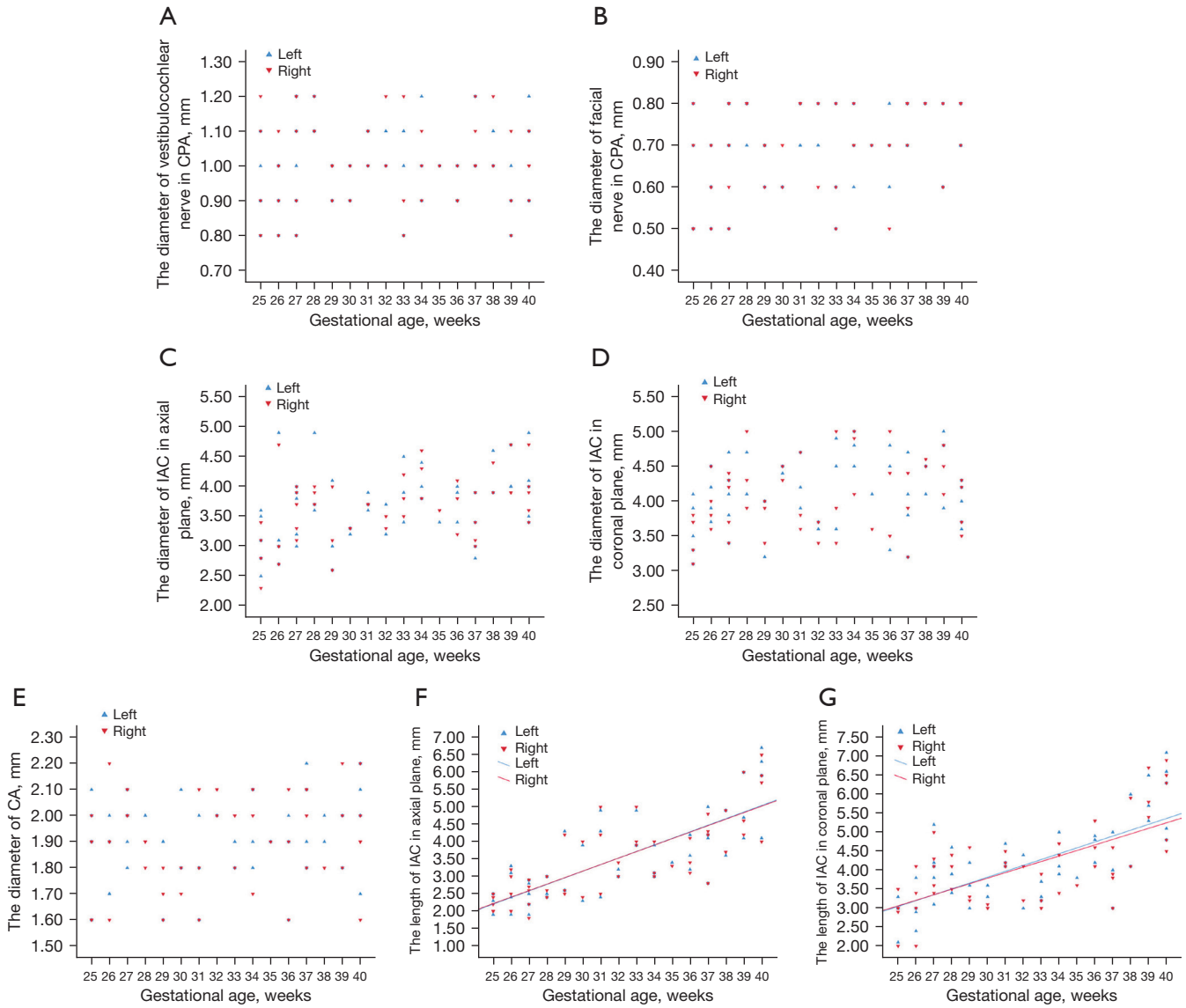

Figure 6 Scatterplots showing the relationship between the measurement of each cochlear nerve-related structure and gestational age in weeks. (A) The diameter of the vestibulocochlear nerve in the CPA. (B) The diameter of the facial nerve in the CPA (C). The diameter of the IAC in the axial plane. (D) The diameter of the IAC in the coronal plane. (E) The diameter of the CA. (F) The length of the IAC in the axial plane. (G) The length of the IAC in the coronal plane. In the scatterplots, the blue triangles represent males, and the green triangles represent females. CPA, cerebellopontine angle; IAC, internal auditory canal; CA, cochlear aperture; GA, gestational age.

obtained on the day of pregnancy termination (27). Finally, in this study, the 3.0 Tesla MRI system was used to measure fetal specimens in the second and third trimesters of pregnancy at approximately 26 ℃. Intrauterine fetal MRI is usually performed after 25 weeks of gestation, following the completion of fetal inner ear development. By incorporating these various measures to minimize differences between the specimens and the living fetuses, we aimed to ensure the accuracy and reliability of the findings of this study. We anticipated that the 3D T2-SPACE sequence used for inner ear imaging in this study would capture fine anatomical details.

Several reasons have been proposed as to why the cochlear nerve is not clearly visible on MRI (2), including

Table 2 MRI measurements of each structure

Cochlear nerve-related structures	Measured parameters	Average value, mean ± SD	ICC value
Vestibulocochlear nerve	Diameter in the CPA (mm)	1.00±0.14	0.89
Facial nerve	Diameter in the CPA (mm)	0.70±0.13	0.88
Vestibulocochlear nerve: facial nerve	Ratio of the diameter	1.46±0.13	–
IAC	Diameter in the axial plane (mm)	3.64±0.57	0.94
	Length in the axial plane (mm)	3.55±1.22	0.93
	Diameter in the coronal plane (mm)	4.07±0.52	0.89
	Length in the coronal plane (mm)	4.12±1.11	0.91
CA	Diameter (mm)	1.90±0.17	0.73

MRI, magnetic resonance imaging; SD, standard deviation; ICC, inter-class correlation coefficient; CPA, cerebellopontine angle; IAC, internal auditory canal; CA, cochlear aperture.

Table 3 MRI measurement results of each structure for the different sides

Cochlear nerve-related structures	Measured parameters	Left, mean ± SD	Right, mean ± SD	P
Vestibulocochlear nerve	Diameter in the CPA (mm)	0.99±0.13	1.00±0.14	0.47
Facial nerve	Diameter in the CPA (mm)	0.69±0.15	0.71±0.13	0.35
Vestibulocochlear nerve: facial nerve	Ratio of the diameter	1.46±0.13	1.47±0.14	–
IAC	Diameter in the axial plane (mm)	3.66±0.61	3.63±0.54	0.2
	Length in the axial plane (mm)	3.54±1.23	3.55±1.22	0.9
	Diameter in the coronal plane (mm)	4.10±0.51	4.05±0.52	0.1
	Length in the coronal plane (mm)	4.14±1.11	4.10±1.1	0.21
CA	Diameter (mm)	1.91±0.16	1.89±0.19	0.38

MRI, magnetic resonance imaging; SD, standard deviation; CPA, cerebellopontine angle; IAC, internal auditory canal; CA, cochlear aperture.

motion artifacts and the obstruction of the nerves by nearby blood vessels and cerebellum structures owing to the partial volume effect. Cochlear nerve dysplasia with IAC or CA stenosis is difficult to detect. Finally, the cochlear nerve may be misaligned with the IAC wall, not separate from the vestibular nerve, or may travel outside the inner auditory canal. Nevertheless, even when cochlear nerve fibers are not visible on MRI, some patients can still benefit from a cochlear implant (28,29). This implies that factors such as the presence of cochlear nerve fibers, the width of the IAC, and the ratio of the diameter of the facial nerve to the vestibulocochlear nerve at the CPA may be associated with long-term hearing thresholds after surgery (29). Moreover, in intrauterine and specimen fetal MRI, the limited resolution can be overcome by indirectly evaluating cochlear nerve development through the imaging of related structures.

The facial nerve and vestibulocochlear nerve exit and enter the CPA anteriorly and posteriorly from the medullary pontine sulcus, respectively, with the facial nerve located anteriorly, and the vestibulocochlear nerve situated posteriorly. Vestibulocochlear nerves are generally 1.5 to 2 times the diameter of facial nerves (30). At the central level of the IAC, the vestibulocochlear nerve is divided into the vestibular and cochlear nerves (2); thus, the vestibulocochlear nerve diameter can be used as a proxy measure for cochlear nerve development (14). When the diameter of the cochlear nerve is smaller than that of the facial nerve, the specificity of diagnosing cochlear nerve deficiency is higher. Many researchers have measured the facial, cochlear, superior vestibular, and inferior vestibular nerves (31-34) in the IAC. In one study, at the point nearest

to the fundus of the IAC where the margin of the cochlear nerve and facial nerve could be identified, the mean long and short diameters of the cochlear nerve were 1.35±0.16 and 0.99±0.18 mm, respectively, while the mean values of the facial nerve were 1.18±0.17 and 0.87±0.16 mm (31). Another study reported that at the IAC fundus, the diameters were 1.00±0.03 mm (facial nerve), 1.03±0.04 mm (cochlear nerve), 0.98±0.04 mm (superior vestibular nerve), and 0.71±0.03 mm (inferior vestibular nerve) (32). Additionally, another study reported that in the middle of the IAC, the vertical and horizontal diameters of the cochlear nerve in normal hearing ears were 1.10±0.21 and 1.11±0.20 mm, respectively, while the facial nerve diameters were 0.95±0.21 and 1.03±0.22 mm, respectively (33). A study of normal hearing children reported that the mean diameters of the cochlear nerve at the midpoint of the IAC, IAC fundus, and CA were 1.12±0.08, 1.05±0.06, and 0.87±0.14 mm, respectively (34). In the present study, we measured the diameters in the parasagittal images perpendicular to the nerves in the CPA, but no significant differences were found between the right and left sides. The diameter of the vestibulocochlear nerve was 1.00±0.14 mm and that of the facial nerve was 0.70±0.13 mm in the CPA. Due to factors such as the measurement location, race, scanning sequence, measuring method, and selection of research techniques, our findings are slightly lower than those previously reported. Nevertheless, our results suggest that nerves in the CPA may continue to grow after birth, which merits further investigation. We also found that the ratio of the diameter of the vestibulocochlear nerve to that of the facial nerve in the CPA was 1.47±0.10, which is consistent with previously reported values (30). Moreover, the size of the ratio was significantly correlated with the effectiveness of the cochlear implants (29,35).

The classical embryological theory (36) states that before the formation of the IAC (before 24 weeks of gestation), hypoplasia of the cochlear nerve leads to the inadequate inhibition of IAC ossification, resulting in stenosis of the IAC. After IAC formation (after 24 weeks of gestation), neurotrophin is required for the development of the cochlear nerve. Neurotrophin deficiency can cause nerve degeneration but will not affect the size of the IAC. Consequently, the IAC remains normal despite cochlear nerve hypoplasia (37). Stenosis is associated with IAC and dysplasia of the cochlear nerve (16,17,37). Further, it has been suggested that the diameter of the IAC indirectly reflects the development of the cochlear nerve. In the present study, the gestational period ranged from 25 to 40 weeks. At this stage, IAC ossification has been completed and the IAC can be clearly visualized. An evaluation of IAC development can be achieved by measuring the diameters and lengths of the IAC in both the axial and coronal planes, respectively. We observed various types of IAC morphology, including parallel, flared, and ampulla tubes. The IAC fundus is divided into two parts containing slim nerves at the CA level, one part leading to the cochlea and the other to the vestibule. In addition, the IAC varied greatly in length (1.9–7.1 mm) and increased linearly with GA. IAC length in normal adults is approximately 9.9 mm (8–13 mm) with an anteroposterior diameter of 5.9 mm (4–8 mm) (38), which suggests that the IAC continues to grow from the middle and late stages of pregnancy to the onset of labor (12). The diameter of the IAC at the porus acusticus internus was reported to be approximately 5.5±1.1 mm (17), while the anteroposterior and craniocaudal diameters in the middle of the IAC on axial and coronal sections were reported to be approximately 5.93±0.25 and 5.70±0.26 mm, respectively (39). In the present study, the vertical and transverse diameters of the IAC were 3.64±0.57 and 4.07±0.52 mm, respectively, and no significant differences were observed between the sides. The measured values reported in this study are smaller than those reported in previous studies (17,38,39). This discrepancy might be due to the growth of the IAC after the completion of ossification at 24 weeks of gestation (12), or to the highly variable shape of the IAC, which results in inconsistent measurement levels and locations.

The CA refers to the bony canal between the bottom of the IAC and the base of the modiolus where the cochlear nerve is located. Its diameter has previously been measured in normal individuals. For example, Henderson *et al.* (40) evaluated histopathologic axial sections from normal human temporal bones and found that the mean CA diameter was 2.26±0.25 mm. They also found no significant differences between the participants in terms of age and sex. Stjernholm *et al.* (41) examined the diameter of the CA in normal adults using computed tomography (CT) examinations and reported that it was approximately 1.91 mm. The CA is primarily measured by CT; however, this involves ionizing radiation, which limits its application to fetuses. Alternatively, the fetal CA can be clearly defined using MRI. In general, our findings are consistent with previous research findings that indicate the width of the CA is approximately 1.90±0.17 mm and does not differ significantly between the two sides. However, our results were lower than those reported in a histological study (40), which may be related to differences

in the measurement methods. The mechanism of CA dysplasia and cochlear nerve dysplasia remains unclear; however, it has been speculated that it may be similar to IAC stenosis. Several studies have shown that the diameter of the CA can be used to accurately predict the development of the cochlear nerve (17-19) and is more sensitive than the diameter of the IAC.

To the best of our knowledge, this study is the first to establish a reference range from an imaging perspective. Additionally, the appearance time and change rule of some structures, as determined by imaging methods, are inconsistent with classical embryology. For example, this may occur when a partial cranial sulcus appears in a fetus (42,43). Therefore, the use of precise data in this study further validated the classical embryological theory. In addition, this study did not group the subjects based on GA and sex, nor did it compare a postnatal population with a prenatal population. This is mainly because the bony labyrinth of the inner ear is fully developed during the second and third trimesters of pregnancy, and thus age does not alter the main relevant diameters (12). Additionally, the limited number of specimens and uneven distribution of the male and female fetuses might have contributed to this finding. No significant sex differences in these structures have been reported among fetuses and infants.

With the high-resolution 3D T2-SPACE sequence, it is possible to clearly illustrate the anatomical structure of the inner ear, measure the relevant diameters of the cochlear nerve, and then outline the normal range of fetal inner ear development in the second and third trimester. Our findings provide a framework for evaluating the development of the cochlear nerve clinically.

Conclusions

Normative measurements of structures related to cochlear nerve development in fetuses can provide relevant information for the evaluation of cochlear nerve development itself. These data can then be applied to guide clinical evaluations regarding the development of the cochlear nerve.

Acknowledgments

Funding: The study was supported by the National Natural Science Foundation of Shandong Province (No. ZR2021MH216), and the Shandong Medical and Health Science and Technology Development Plan (No. 202109010865).

Footnote

Conflicts of Interest: All authors have completed the ICMJE uniform disclosure form (available at https://qims.amegroups.com/article/view/10.21037/qims-24-626/coif). C.A.M. serves as an unpaid editorial board member of *Quantitative Imaging in Medicine and Surgery*. The other authors have no conflicts of interest to declare.

Ethical Statement: The authors are accountable for all aspects of the work, including ensuring that any questions related to the accuracy or integrity of any part of the work have been appropriately investigated and resolved. The parents provided informed consent for the donation of the fetal cadavers. The study protocol was approved by the Ethics Committee at the School of Medicine, Shandong University (No. SDULCLL2021-1-05). The study was conducted in accordance with the Declaration of Helsinki (as revised in 2013).

References

1. Minami SB, Yamamoto N, Hosoya M, Enomoto C, Kato H, Kaga K. Cochlear Implantation in Cases of Inner Ear Malformation: A Novel and Simple Grading, Intracochlear EABR, and Outcomes of Hearing. Otol Neurotol 2021;42:e117-23.
2. Freeman SR, Sennaroglu L. Management of Cochlear Nerve Hypoplasia and Aplasia. Adv Otorhinolaryngol 2018;81:81-92.
3. He S, Chao X, Wang R, Luo J, Xu L, Teagle HFB, Park LR, Brown KD, Shannon M, Warner C, Pellittieri A, Riggs WJ. Recommendations for Measuring the Electrically Evoked Compound Action Potential in Children With Cochlear Nerve Deficiency. Ear Hear 2020;41:465-75.
4. Isaacson G, Mintz MC. Prenatal sonographic visualization of the inner ear. J Ultrasound Med 1986;5:409-10.
5. Dunn K, Reissland N, Reid VM. The functional foetal

brain: A systematic preview of methodological factors in reporting foetal visual and auditory capacity. Dev Cogn Neurosci 2015;13:43-52.
6. Moreira NC, Teixeira J, Raininko R, Wikstrom J. The ear in fetal MRI: what can we really see? Neuroradiology 2011;53:1001-8.
7. Katorza E, Nahama-Allouche C, Castaigne V, Gonzales M, Galliani E, Marlin S, Jouannic JM, Rosenblatt J, le Pointe HD, Garel C. Prenatal evaluation of the middle ear and diagnosis of middle ear hypoplasia using MRI. Pediatr Radiol 2011;41:652-7.
8. Ohtsuki S, Ishikawa A, Yamada S, Imai H, Matsuda T, Takakuwa T. Morphogenesis of the Middle Ear during Fetal Development as Observed Via Magnetic Resonance Imaging. Anat Rec (Hoboken) 2018;301:757-64.
9. Zhang X, Zheng W, Feng Y, Yu N, Qin J, Li K, Yan G, Zou Y, Li B. The role of MRI in the prenatal diagnosis and classification of fetal microtia. Eur Radiol 2023;33:7707-15.
10. Millischer AE, Sonigo P, Attie T, Spaggiari E, O'Gorman N, Bessieres B, Kermorvant E, Boddaert N, Salomon LJ, Grevent D. Fetal MRI findings in a retrospective cohort of 26 cases of prenatally diagnosed CHARGE syndrome individuals. Prenat Diagn 2019;39:781-91.
11. Tilea B, Garel C, Menez F, Vuillard E, Elmaleh-Bergès M, Delezoide AL, Sebag G. Contribution of fetal MRI to the diagnosis of inner ear abnormalities: report of two cases. Pediatr Radiol 2006;36:149-54.
12. Nemzek WR, Brodie HA, Chong BW, Babcook CJ, Hecht ST, Salamat S, Ellis WG, Seibert JA. Imaging findings of the developing temporal bone in fetal specimens. AJNR Am J Neuroradiol 1996;17:1467-77.
13. Isaacson G, Mintz MC, Sasaki CT. Magnetic resonance imaging of the fetal temporal bone. Laryngoscope 1986;96:1343-6.
14. Yamazaki H, Leigh J, Briggs R, Naito Y. Usefulness of MRI and EABR Testing for Predicting CI Outcomes Immediately After Cochlear Implantation in Cases With Cochlear Nerve Deficiency. Otol Neurotol 2015;36:977-84.
15. Naguib NNN, Hey C, Shaaban MS, Elabd AM, Hassan HHM, Gruber-Rouh T, Kaltenbach B, Harth M, Ackermann H, Stöver T, Vogl TJ, Nour-Eldin NA. Assessment of the cochlear nerve to facial nerve size ratio using MR multiplanar reconstruction of the internal auditory canal in patients presenting with acquired long-standing hearing loss. Br J Radiol 2017;90:20160870.
16. Kim H, Kim DY, Ha EJ, Park HY. Clinical Value of Measurement of Internal Auditory Canal in Pediatric Cochlear Implantation. Ann Otol Rhinol Laryngol 2019;128:61S-8S.
17. Bächinger D, Breitsprecher TM, Pscheidl A, Dhanasingh A, Mlynski R, Dazert S, Langner S, Weiss NM. Internal auditory canal volume in normal and malformed inner ears. Eur Arch Otorhinolaryngol 2023;280:2149-54.
18. Sorge M, Sorge I, Pirlich M, Fuchs M, Meuret S, Hirsch FW, Dietz A, Gräfe D. Diameter of the Cochlear Nerve Canal predicts Cochlear Nerve Deficiency in Children with Sensorineural Hearing Loss. Rofo 2022;194:1132-9.
19. Chung J, Jang JH, Chang SO, Song JJ, Cho SW, Kim SY, Lee JH, Oh SH. Does the Width of the Bony Cochlear Nerve Canal Predict the Outcomes of Cochlear Implantation? Biomed Res Int 2018;2018:5675848.
20. Zhang S, Yuan X, Peng Z, Jian N, Tian M, Feng X, Lin X, Wang X. Normal fetal development of the cervical, thoracic, and lumbar spine: A postmortem study based on magnetic resonance imaging. Prenat Diagn 2021;41:989-97.
21. Jian N, Tian MM, Xiao LX, Zhao H, Shi Y, Li G, Zhang S, Lin XT. Normal development of sacrococcygeal centrum ossification centers in the fetal spine: a postmortem magnetic resonance imaging study. Neuroradiology 2018;60:821-33.
22. Yuan L, Lv B, Wang H, Wang Z, Shang H, Li X, Liang L, Lin X. T2-weighted Imaging Features of the Fetal Thymus in the Middle and Late Pregnancy: A Post-mortem Study based on Magnetic Resonance Imaging. Curr Med Imaging 2024. [Epub ahead of print]. doi: 10.2174/0115734056282196240105060732.
23. Miao M, Lin X, Zhang Z, Zhao H. Normal development of the fetal spinal canal and spinal cord at T12 on 3.0-T MRI. Acta Radiol 2019;60:623-7.
24. Kobayashi T, Shiotani S, Kaga K, Saito H, Saotome K, Miyamoto K, Kohno M, Kikuchi K, Hayakawa H, Homma K. Characteristic signal intensity changes on postmortem magnetic resonance imaging of the brain. Jpn J Radiol 2010;28:8-14.
25. Ruder TD, Hatch GM, Siegenthaler L, Ampanozi G, Mathier S, Thali MJ, Weber OM. The influence of body temperature on image contrast in post mortem MRI. Eur J Radiol 2012;81:1366-70.
26. Birkl C, Langkammer C, Golob-Schwarzl N, Leoni M, Haybaeck J, Goessler W, Fazekas F, Ropele S. Effects of formalin fixation and temperature on MR relaxation times in the human brain. NMR Biomed 2016;29:458-65.
27. Verhoye M, Votino C, Cannie MM, Segers V, Mabiglia C, Cos T, Lipombi D, Jani JC. Post-mortem high-field

magnetic resonance imaging: effect or various factors. J Matern Fetal Neonatal Med 2013;26:1060-5.
28. Wei X, Li Y, Chen B, Gong Y, Fu QJ, Liu T, Cui D, Su Q, Shi Y. Predicting Auditory Outcomes From Radiological Imaging in Cochlear Implant Patients With Cochlear Nerve Deficiency. Otol Neurotol 2017;38:685-93.
29. Luo JF, Chao XH, Wang RJ, Liu XM, Xu QA, Fan ZM, Xu L, Wang HB. The imaging characteristics and prognosis of patients with cochlear implants whose cochlear nerves are not shown on MRI. Zhonghua Er Bi Yan Hou Tou Jing Wai Ke Za Zhi 2021;56:1283-91.
30. Casselman JW, Offeciers FE, Govaerts PJ, Kuhweide R, Geldof H, Somers T, D'Hont G. Aplasia and hypoplasia of the vestibulocochlear nerve: diagnosis with MR imaging. Radiology 1997;202:773-81.
31. Nakamichi R, Yamazaki M, Ikeda M, Isoda H, Kawai H, Sone M, Nakashima T, Naganawa S. Establishing normal diameter range of the cochlear and facial nerves with 3D-CISS at 3T. Magn Reson Med Sci 2013;12:241-7.
32. Wang B, Xian JZ, Niu YT, Zhao B, Wang ZC. Study of normal anatomy of internal auditory canal fundus with CT and MRI. Radiol Pract 2008;9:950-4.
33. Kang WS, Hyun SM, Lim HK, Shim BS, Cho JH, Lee KS. Normative diameters and effects of aging on the cochlear and facial nerves in normal-hearing Korean ears using 3.0-tesla magnetic resonance imaging. Laryngoscope 2012;122:1109-14.
34. Lou J, Gong WX, Wang GB. Cochlear nerve diameters on multipoint measurements and effects of aging in normal-hearing children using 3.0-T magnetic resonance imaging. Int J Pediatr Otorhinolaryngol 2015;79:1077-80.
35. Chao X, Luo J, Fan Z, Shi H, Han Y, Wang R, Song Y, Wang G, Wang H, Xu L. Usefulness of radiological findings for predicting cochlear implantation outcomes in children with cochlear nerve deficiency: a pilot study. Acta Otolaryngol 2016;136:1051-7.
36. Feraco P, Piccinini S, Gagliardo C. Imaging of inner ear malformations: a primer for radiologists. Radiol Med 2021;126:1282-95.
37. El Sadik AO, Shaaban MH. The relationship between the dimensions of the internal auditory canal and the anomalies of the vestibulocochlear nerve. Folia Morphol (Warsz) 2017;76:178-85.
38. Amjad AH, Scheer AA, Rosenthal J. Human internal auditory canal. Arch Otolaryngol 1969;89:709-14.
39. Erkoç MF, Imamoglu H, Okur A, Gümüş C, Dogan M. Normative size evaluation of internal auditory canal with magnetic resonance imaging: review of 3786 patients. Folia Morphol (Warsz) 2012;71:217-20.
40. Henderson E, Wilkins A, Huang L, Kenna M, Gopen Q. Histopathologic investigation of the dimensions of the cochlear nerve canal in normal temporal bones. Int J Pediatr Otorhinolaryngol 2011;75:464-7.
41. Stjernholm C, Muren C. Dimensions of the cochlear nerve canal: a radioanatomic investigation. Acta Otolaryngol 2002;122:43-8.
42. Nishikuni K, Ribas GC. Study of fetal and postnatal morphological development of the brain sulci. J Neurosurg Pediatr 2013;11:1-11.
43. Zhang Z, Hou Z, Lin X, Teng G, Meng H, Zang F, Fang F, Liu S. Development of the fetal cerebral cortex in the second trimester: assessment with 7T postmortem MR imaging. AJNR Am J Neuroradiol 2013;34:1462-7.

Cite this article as: Zhao H, Sun L, Xiao L, Wang L, Hu N, Miao M, Ginat DT, Mallio CA, Lin X. A postmortem high-resolution MRI study of the development of cochlear nerve-related structures in the second and third trimesters of pregnancy. Quant Imaging Med Surg 2024;14(9):6325-6336. doi: 10.21037/qims-24-626

